



A Cellular Automata Based Rainfall-Runoff Model for Urban Inundation Analysis Under Different Land Uses

Shuang Yao¹ · Nengcheng Chen^{1,2} · Wenying Du¹ · Chao Wang¹ · Cuizhen Chen³

Received: 23 November 2020 / Accepted: 31 March 2021 / Published online: 13 April 2021
© The Author(s), under exclusive licence to Springer Nature B.V. 2021

Abstract

Recently many runoff models based on cellular automaton (CA) have been developed to simulate floods; however, the existing models cannot be readily applied to complex urban environments. This study proposes a novel rainfall-runoff model based on CA (RRCA) to simulate inundation. Its main contributions include a fine runoff generation process that considers 12 urban scenarios rather than a single land use type and the confluence process determined by the new transition rules considering water supply and demand (WS-WD transition rules). RRCA was compared with another CA based flood model (E2DCA). With the benchmark model, the results showed that there was good agreement, with an R-squared greater than 0.9, and that RRCA was more sensitive to waterlogging levels than E2DCA. Furthermore, the simulated vegetation interception, infiltration and drainage processes had varying degrees of impact on waterlogging. Corresponding measures can be taken in urban flood management according to the identification of areas experiencing drainage difficulties.

Keywords Accurate flood simulation · Cellular automata · Inundation analysis · Land use

1 Introduction

Urban floods occur frequently as urbanization processes accelerate. Hence, flood-prone cities are increasingly challenged to mitigate the impact of urban waterlogging (Alves et al. 2020). Flood models are an effective approach to obtain flood information and provide insights into flood management (Jamali et al. 2018).

In general, flood models can be divided into three categories: empirical methods, simplified methods and hydrodynamic models (Teng et al. 2019). Empirical methods obtain flood information by processing the observation data, such as evaluating remote sensing images for flood mapping (Domeneghetti et al. 2019). Simplified methods simulate floods

✉ Wenying Du
duwenying@whu.edu.cn

¹ State Key Laboratory of Information Engineering in Surveying, Mapping and Remote Sensing, Wuhan University, 129 Luoyu Road, Wuhan 430079, China

² Collaborative Innovation Center of Geospatial Technology, Wuhan, China

³ Institute of Water Science Research in Wuhan, Wuhan, China

without involving the hydraulic process of inundation, such as the rapid flood spreading method (Lhomme et al. 2008). However, these models are limited by their weak dynamic effects. Hydrodynamic models involving hydrologic and hydraulic processes can obtain more accurate results based on numerous parameters and high computational demands (Teng et al. 2017). Therefore, the application of the hydrodynamic model is limited in complex environments with a low computing capacity (Vu et al. 2019). As a simple 2D flood model, a model based on cellular automaton (CA) has recently become of focus (Gregorio and Serra 1999). It has fewer parameters and can simulate inundation processes with a similar accuracy or a slightly lower accuracy than other hydrodynamic models (Manfreda and Samela 2019).

A typical CA-based model is a discrete dynamic system and includes a lattice of cells covering the study area. The CA system defines local neighborhoods, cell state attributes, and transition rules determining the changes in cell properties (Wolfram 1984). Considering the confluence process in flood evolution, i.e., the process of runoff concentration in a catchment, CA does well when simulating the flow exchange occurring among units. Therefore, CA can provide insights into the dynamic development of inundation by combining the physical processes involved in surface runoff production and confluence (Jamali et al. 2019). Liu et al. (2015) ensured the stability of the flood simulation by changing the calculation method of time step in the model based on CA. Armal and Al-Suhili (2019) developed a CA-based model for the inundation extent simulation of flash floods in an urban catchment.

CA-based models have the advantages of a high speed and fewer parameter requirements and is usually used to simulate floods in river basins (Guidolin et al. 2016). However, due to the increasing complexity of the urban environment, most CA-based models have difficulty simulating the development of urban waterlogging, especially fine simulations with a small range. In addition, CA models only divide the underlying surface into pervious and impervious areas for runoff calculations, and the treatment of water circulation is divorced from reality (Liu et al. 2015). In fact, the layout of buildings and drainage facilities in cities will have an impact on the waterlogging.

In the case of floods, especially in the absence of hydrological data, the rapid inundation analysis can identify key points in time to make effective emergency management decisions (Tyler et al. 2019). The study of surface runoff affected by various land use types is useful in the identification of the causes and development of floods (Shang et al. 2019).

Consequently, this study proposes a novel rainfall-runoff model based on CA (RRCA) for inundation simulation and analysis. Different runoff generation processes involving vegetation interception, roof storage, infiltration, depression storage, drainage or the combination of the above, are used to determine the submerged depth per unit area. Moreover, new WS-WD transition rules in the confluence process are obtained by the relationship between the water supply and demand, which simulates the inundation process more accurately.

2 Model Development

RRCA incorporates runoff generation and confluence processes and considers the complex urban environment and water exchange rules to realize the accurate simulation of inundation processes. The procedure is shown in Fig. 1.

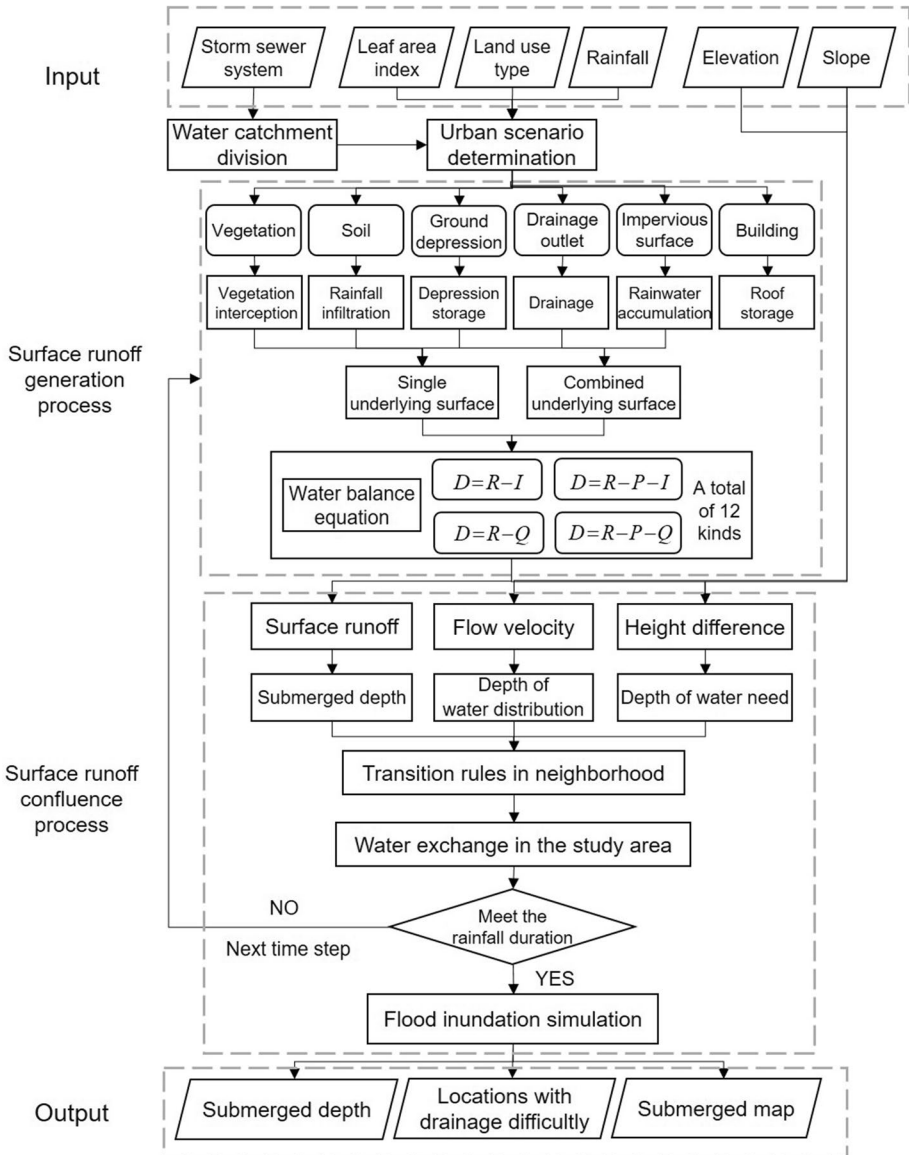


Fig. 1 The procedure of urban flood simulation by the rainfall-runoff model based on CA (RRCA)

The RRCA model consists of four parts shown in Fig. 1. Six kinds of data act as inputs for RRCA. The runoff generation process depends on the land use types and urban scenarios used to determine the submerged state of each cell. The confluence process is constrained by transition rules among cells. The submerged depth, submerged map and locations with drainage difficulty are the outputs used to provide decision support for flood management.

2.1 Division of Water Catchment

Due to the dynamic framework of CA, with its discrete time, space and state processing, it can effectively shorten the simulation run time by dividing the area into several catchments and performing parallel simulations (Guidolin et al. 2012). Moreover, the flooding simulation is conducted in each catchment, reducing the influence of water outside the area flowing into the catchment. Considering the small changes in the terrain slope of urban neighborhoods, the catchment division in this study is mainly based on the distribution of drainage facilities. The catchments are divided with the Voronoi method based on drainage networks (Li et al. 2020). Each catchment includes at least one main drainage outlet, and is adjusted slightly according to the terrain elevation and road distribution.

2.2 Runoff Generation Considering Combination Scenarios

2.2.1 Runoff Loss on Single Land Use Type

Rainfall interception by vegetation is the first step in the procedure to reduce surface runoff. Equation (1) is a vegetation interception volume calculation often used for urban rainfall interception, and the relationship between the maximum interception and the leaf area index is shown in Eq. (2) (Nazari et al. 2020):

$$P = P_{\max}[1 - \exp(-0.046LAI/P_{\max})] \quad (1)$$

$$P_{\max} = 0.935 + 0.498LAI + 0.00575LAI^2 \quad (2)$$

where P is the cumulative interception (mm), P_{\max} is the maximum interception (mm), R is the cumulative rainfall (mm), and LAI is the leaf area index.

Rainwater accumulates on the roof when the underlying surface is a building. Water exceeding the roof limit will flow to the ground, and the redundant runoff is calculated by the runoff coefficient method (Rossman and Huber 2015):

$$B = ciA \quad (3)$$

where B is the runoff volume after the roof is filled with rain (m^3), c is the runoff coefficient, i is the amount of rainfall (m), and A is the roof area (m^2).

Rainfall infiltration is another cause of runoff loss (Morbidei et al. 2018). Horton (1940) proposed an infiltration model with a simple structure and fewer parameters to estimate the water infiltration rate (Almeida et al. 2018):

$$I = I_c + (I_0 - I_c) \exp(-kt) \quad (4)$$

where I is the infiltration rate at time t (mm/h), I_c is the steady infiltration rate (mm/h), I_0 is the initial infiltration rate (mm/h), and k is the decay parameter of the infiltration curve.

When the rainfall intensity is greater than the infiltration capacity, the rainfall beyond the infiltration volume forms surface water and accumulates in ground depressions. The depression volume is calculated considering ground elevation in the Moore-neighborhood (Uguz et al. 2016). This study uses a simple algorithm to quickly calculate depression storage. First, a center cell is determined. The height difference between the center cell and eight adjacent cells is calculated. Then, whether the water depth accumulated

on the center cell D_c is greater than the minimum height difference Δh_{\min} is determined. If this is true, then the center cell will not have depression storage at the subsequent moment. Otherwise, the depression storage DS_c will be $DS_c = \Delta h_{\min} - D_c$.

In addition, the drainage capacity of a rainwater grate has been proposed by Sun (1999):

$$Q = \begin{cases} iA & 0 < h \leq 0.01 \\ AC\sqrt{2gh}K & h > 0.01 \end{cases} \tag{5}$$

where Q is the drainage flow rate (m^3/s), i is the rainfall rate (m/s), A is the area of rainwater grate (m^2), C is the orifice coefficient, g is the gravitational acceleration, h is the water depth on the rainwater grate (m), and K is the orifice obstruction coefficient.

2.2.2 Surface Runoff Generation in Different Scenario Combinations

The evaporation process is negligible in this study, because evaporation loss is small during rainfall (Zhang and Pan 2014). According to the water balance equation (Zeng et al. 2012), the submerged depth D resulting from surface runoff is calculated as follows:

$$D = R - WL \tag{6}$$

where R is the rainfall, and WL is the water loss in the surface water circulation.

The initial submerged depth obtained from the runoff generation process varies according to the land use types. We consider a complex environment, and specifically account for the fact that plants usually overlap with other types of underlying surfaces. Therefore, the calculation of submerged depth considers not only the land use type, but also the combination of various water loss processes. There are 12 scenarios included in the submerged depth calculation:

Building	$D=R-B$
Impervious surface	$D=R$
Impervious depression	$D=R-DS$
Soil	$D=R-I$
Soil and depression	$D=R-I-DS$
Rainwater grate	$D=R-Q$
Vegetation and building	$D=R-P-B$
Vegetation and impervious surface	$D=R-P$
Vegetation and impervious depression	$D=R-P-DS$
Vegetation and soil	$D=R-P-I$
Vegetation, soil and depression	$D=R-P-I-DS$
Vegetation and rainwater grate	$D=R-P-Q$

The runoff generation process occurs in each cell of equal size, so we divide the above water volume by the unit cell area to obtain the water depth for calculation. D is the submerged depth of surface runoff, R is the rainfall, B is the runoff depth after the roof is filled with rain, DS is the depth of the depression storage, I is the depth of the infiltration volume, Q is the depth of the drainage volume, and P is the depth of the interception volume.

2.3 WS-WD Transition Rules

After determining the initial submerged depth of each cell by the above processes, the algorithm must determine how water exchange occurs among cells due to the topography and transition rules considering water supply and demand, thereby changing the submergence state of neighborhood, and leading to the confluence process in catchments.

The WS-WD transition rules are depicted as follows:

1: Select center cell. The center cell is selected only when the height difference Δh_i between the center cell and the neighbor cell i is positive.

2: Calculate the water supply of the center cell and the water demand of neighboring cells. The water supply of the center cell mainly depends on the flow velocity v_{f_i} (Eq. (9)). The water demands of neighboring cells N_i and N_c mainly depend on the height difference (Eq. (11) and Eq. (12)).

3: Compare v_{f_i} , N_c , and the water depth of the center cell to determine the volume of water exchange and then update the water depth D_c of the center cell and water depth D_i of neighboring cell i . Since the unit time steps of all water depth and flow velocity changes are consistent, the values of depth and velocity can be directly compared within each time step.

When $\sum v_{f_i} \geq D_c$,
 if $D_c = N_c$, then $D_c = D_c - N_c$, $D_i = D_i + N_i$
 else, $D_c = 0$, $D_i = D_i + C_i$ (C_i is shown in Eq. (10))
 When $\sum v_{f_i} < D_c$,
 if $\sum v_{f_i} \geq N_c$, then $D_c = D_c - N_c$, $D_i = D_i + N_i$
 else, $D_c = D_c - \sum v_{f_i}$, $D_i = D_i + v_{f_i}$

4: Select another center cell in the next time step. The neighboring cell with the smallest height is selected as the center cell in the next time step, and the above processes are repeated until the final time step.

According to Manning’s formula (Hergarten and Neugebauer 1997), the water flow velocity from the center cell to the neighboring cell i is calculated by Eq. (7). The flow time is calculated by Eq. (8).

$$v_i = \frac{1}{n} h_i^{\frac{2}{3}} s^{\frac{1}{2}} \tag{7}$$

$$t_i = TD/v_i \tag{8}$$

where v_i is the flow velocity (m/s), n is Manning’s roughness coefficient, h_i is the water depth of cell i (m), s is the surface slope, t_i is the flow time (s), and TD is the flow travel distance (m). Since the neighborhood is defined as a Moore neighborhood, the distance between the center cell and its four adjacent cells in the up, down, left and right directions is l which equals the cell side length, and the distance from the diagonal directions is $\sqrt{2}l$.

The actual water supply volume needs to be modified by altering the flow velocity (Shao et al. 2015).

$$v_{fi} = \begin{cases} v_i & t_i \leq T \\ v_i T/t_i & t_i > T \end{cases} \tag{9}$$

When the accumulated water of the center cell is insufficient to act as a supply, the exchanged water C_i between the center cell and the neighboring cell i is affected by the flow velocity:

$$C_i = \frac{v_i}{\sum v_i} D_c \quad (10)$$

The water demand N_i of neighboring cell i is determined by the positive height difference Δh_i between the center cell and each neighboring cell:

$$N_i = \frac{\Delta h_i}{\sum \Delta h_i + \Delta h_{\min}} \Delta h_{\min} \quad (11)$$

$$N_c = \frac{\sum \Delta h_i}{\sum \Delta h_i + \Delta h_{\min}} \Delta h_{\min} \quad (12)$$

3 Case Study

3.1 Study Area

The city of Wuhan is located in the eastern part of China and in the middle reaches of the Yangtze River. It has a northern subtropical monsoon climate referring to climate regionalization in China, with abundant rainfall and sufficient heat. The most severe waterlogging event caused by a rainfall accumulation of 676.1 mm in Wuhan occurred in July of 2016. We selected a region (Fig. 2) in Wuhan as the study area.

The study area is located in the Qiaokou district of Wuhan, near the intersection of the Han River and the Yangtze River. Due to its large impervious surface area and inadequate drainage facilities, heavy rainfall frequently causes urban waterlogging.

3.2 Data Used

Land use type and ground elevation (DEM) data were provided by the Wuhan Surveying and Mapping Bureau. The slope data were derived based on a DEM using ArcGIS10.2.2. Leaf area index (LAI) and soil data were obtained from the Geographical Information Monitoring Cloud Platform (<http://www.dsac.cn/>). Rainfall, drainage system and historical waterlogging data were provided by the Institute of Water Science Research in Wuhan.

The land use type, DEM, slope and LAI were preprocessed to unify the spatial resolution to one meter. Each cell formed a square with a side length of one meter. Rainfall data from 20:00 on July 5, 2016 to 1:00 on July 6, 2016 were selected as input. The temporal resolution of the rainfall data was one minute, as was the simulation time step. The Manning coefficients of impervious surfaces, roads, vegetation and soil are 0.03, 0.012, 0.24, and 0.05, respectively (Engman 1986; McCuen et al. 1996), and the runoff coefficient of building roofs is 0.95 (Fassman-Beck et al. 2016). Based on the soil properties of the study area, the values of the parameters I_c , I_0 , and k in the Horton formula refer to the research of Mishra et al. (2003).

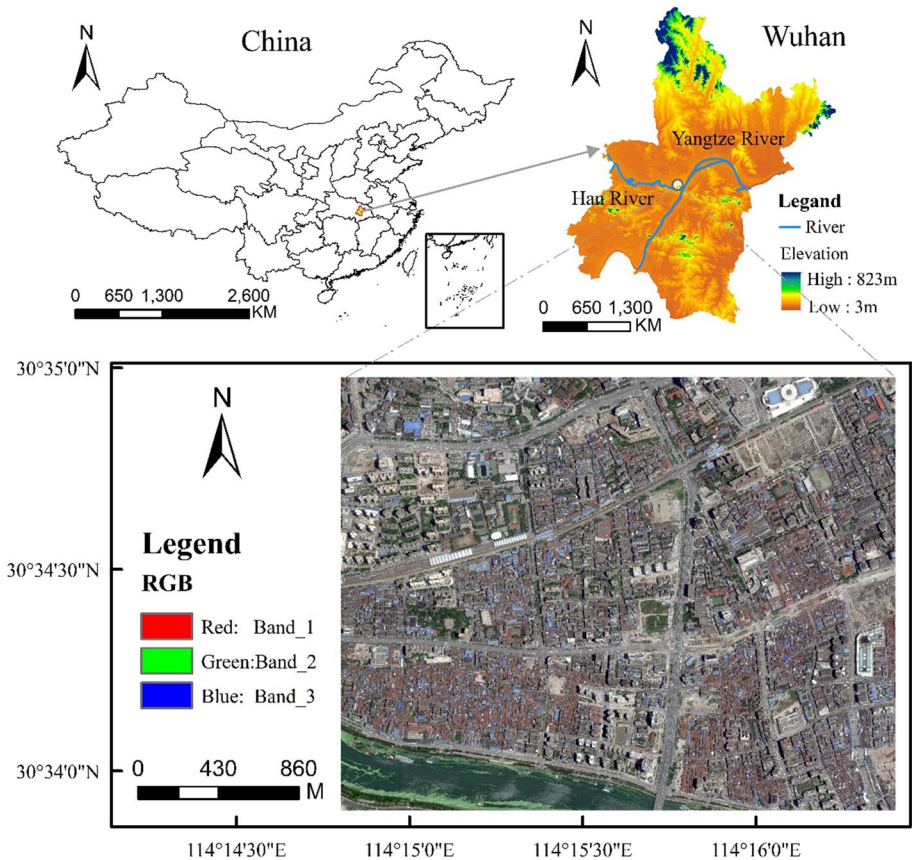


Fig. 2 The location map of the study area

3.3 Model Validation and Comparison

Infoworks Integrated Catchment Management (Infoworks ICM) is a widely used 2D hydraulic commercial software (Innovyze 2012). The urban flood model of Infoworks ICM can fully simulate the urban rainfall runoff process (Bertsch et al. 2017). The results of RRCA which has been calibrated and Infoworks ICM were compared to evaluate our model quantitatively. Moreover, the E2DCA model proposed by Liu et al. (2015) was used as a comparison.

According to the obstruction degree of stagnant water to traffic, the Wuhan Water Affairs Bureau divides water depth into four levels. The first level is “no water” when the water depth is 0 mm; the second level is “a little water” when the depth is less than 150 mm; 150 mm–400 mm is the third level with slight waterlogging; and water depths greater than 400 mm constitute the fourth level with severe waterlogging.

There are usually four metrics to characterize model performance: root mean square error (RMSE, Eq. (13)), R-squared (R^2 , Eq. (1)), true positive rate (TPR, Eq. (15)) and false discovery rate (FDR, Eq. (16)) (Bennett et al. 2013). D_i^p is the submerged depth of cell i simulated by Infoworks ICM, D_i^t is the submerged depth of cell i simulated by the test

models, i.e., RRCA and E2DCA, and n is the number of cells. $\overline{D^b}$ is the mean submerged depth of all cells simulated by Infoworks ICM.

$$RMSE = \sqrt{\frac{\sum_{i=1}^n (D_i^b - D_i^t)^2}{n}} \tag{13}$$

$$R^2 = 1 - \frac{\sum_{i=1}^n (D_i^b - D_i^t)^2}{\sum_{i=1}^n (D_i^b - \overline{D^b})^2} \tag{14}$$

$$TPR = TP / (TP + FN) \tag{15}$$

$$FDR = FP / (TP + FP) \tag{16}$$

TPR and FDR were calculated for four waterlogging levels by cell number. True positive (TP) represents the number of cells that both the test model and the Infoworks ICM identified as having the same level. False negative (FN) represents the number of cells that the Infoworks ICM identified as a certain level while the test model identified them as being of other levels. False Positive (FP) is the opposite of FN. One hundred cells were selected after running the simulation for 300 min. Table 1 shows the comparison between test models (RRCA and E2DCA) and Infoworks ICM at six time points.

For the RMSE in Table 1, the error of RRCA is much smaller than that of E2DCA. In the case of R^2 , the values from the comparison of RRCA and Infoworks ICM all exceed 0.9, while the best value from the comparison of E2DCA and Infoworks ICM is 0.87, indicating that there is a better agreement between RRCA and Infoworks ICM. TPR and FDR are used to assess the sensitivity to waterlogging levels. From the comparison of RRCA and Infoworks ICM, all TPRs are greater than 0.85, showing that RRCA can effectively identify different waterlogging levels; the FDR values decrease with time, showing that the simulation of RRCA becomes more accurate with the gradual waterlogging. However, E2DCA has a high error rate for the identification of waterlogging levels.

Although the Infoworks ICM has a high accuracy for simulating inundation, it is difficult to use by ordinary users because of the large number of parameter calibrations. Infoworks ICM can only simulate inundation every five minutes, while RRCA can simulate

Table 1 The metrics for comparison between test models (RRCA and E2DCA) and Infoworks ICM at six time points

Simulated time instants	Infoworks ICM-RRCA				Infoworks ICM-E2DCA			
	RMSE	R ²	TPR	FDR	RMSE	R ²	TPR	FDR
5 min	0 mm	/	1	0	0 mm	/	1	0
95 min	0.12 mm	0.9	0.88	0.27	1.51 mm	0.82	0.72	0.36
110 min	0.56 mm	0.91	0.89	0.18	4.96 mm	0.84	0.83	0.25
120 min	0.82 mm	0.95	0.93	0.11	7.43 mm	0.87	0.8	0.23
230 min	2.45 mm	0.92	0.93	0.08	31.05 mm	0.79	0.79	0.24
00 min	7.29 mm	0.94	0.94	0.09	62.19 mm	0.85	0.83	0.19

inundation every minute. Moreover, the running time of Infoworks ICM is much longer than that of RRCA when taking in the experimental data. Therefore, RRCA performs better in terms of efficiency and accuracy in neighborhood-scale inundation simulations.

4 Results and Discussions

4.1 Inundation Results

Figure 3 shows the distribution of waterlogging levels at six time points when the areas of different waterlogging levels change significantly.

In Fig. 3b, the areas without stagnant water obviously decreased at 94 min. Slight waterlogging occurred at 109 min in Fig. 3c, and the areas of slight waterlogging increased after 118 min in Fig. 3d. Figure 3e shows that severe waterlogging occurred at 229 min, and the inundated areas greatly increased. At 300 min, the water depth of the original slightly waterlogged areas increased, and almost all of these regions became severely waterlogged, as shown in Fig. 3f. The area changes of the four waterlogging levels indicate that once there is continuous and heavy rainfall, waterlogging will gradually occur in the study area, which will eventually result in severe waterlogging.

4.2 Submerged Depth of Different Land Use Types

The Manning coefficient depending on the land use type affects the velocity of flow, and then influences the water volume. Figure 4 shows the submerged depth variations at every five points for each land use type.

The submerged depths of impervious surfaces, road, vegetation and soil had similar trends depending on the amount of accumulated rainfall. Figure 4 shows that the changes

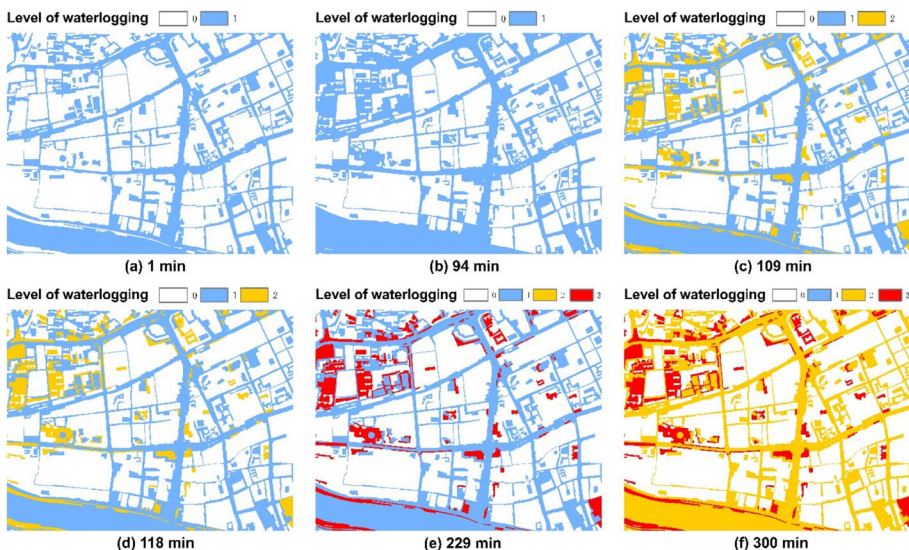


Fig. 3 Distribution map of waterlogging levels at six time points

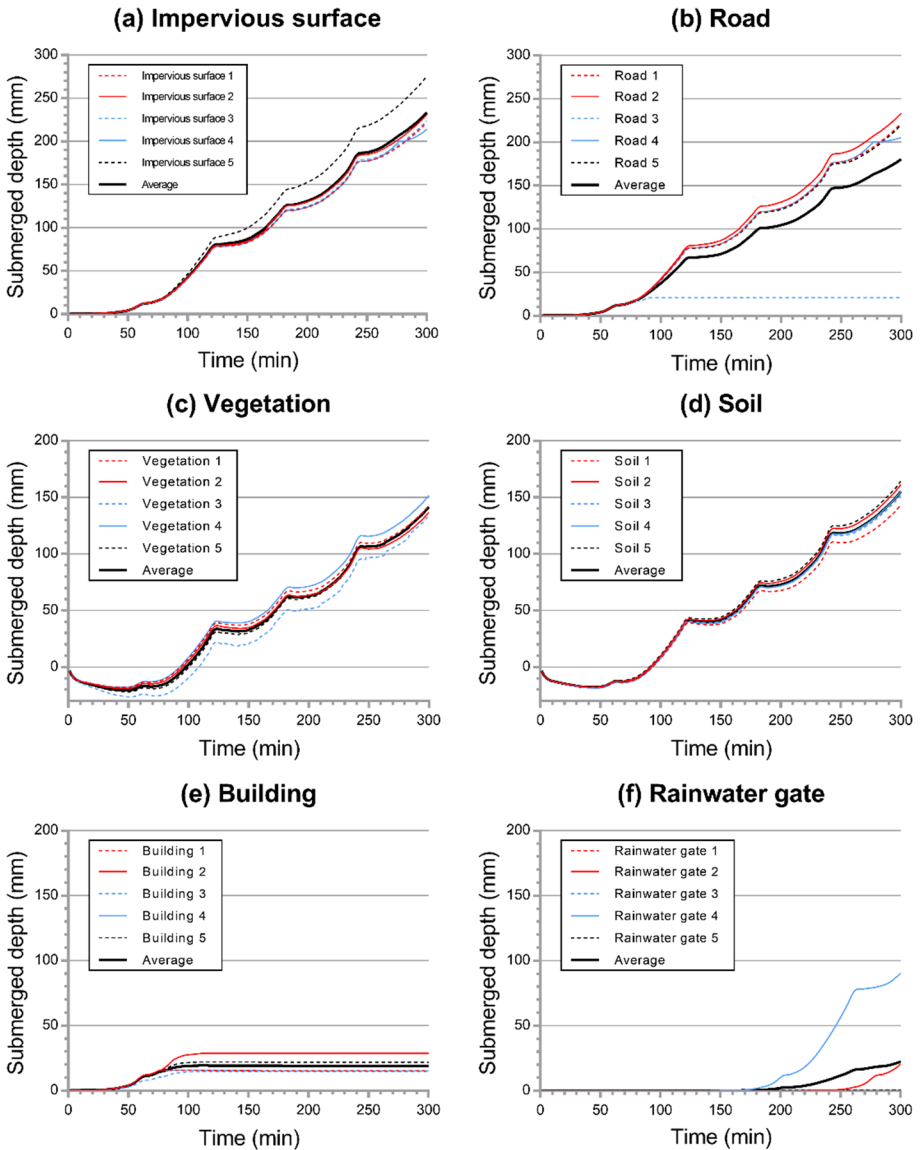


Fig. 4 The submerged depth variation of different land use types. There are five points of each land use type, and the average describes the overall change tendency of submerged depth at every five points

in the submerged depth with each land use type were generally consistent. In general, the average submerged depth of impervious surfaces was greater than that of the other surfaces. Point 5 on the impervious surface had the maximum submerged depth due to the relatively low terrain at this location, as shown in Fig. 4a. There was also an abundance of water on the road, as shown in Fig. 4b. The curve change at point 3 obviously differed from that of other road points, and the water depth was at its minimum. The reason for this is that there is a rainwater gate not far from point 3, and most of the water was drained away.

When there was no surface runoff, the submerged depth was negative, as shown in Fig. 4c and Fig. 4d to analyze whether the accumulated rainfall was less than the water loss. For the vegetation and soil, interception and infiltration took place first and inundation occurred later. In Fig. 4c, the curve changed from declining to rising at approximately 50 min because the total rainfall was greater than the sum of interception and infiltration losses. Stagnant water occurred at approximately 100 min in Fig. 4c. The water volume of vegetation interception mainly depends on the LAI. Due to the sparse vegetation coverage of the study area, vegetation interception had a lesser effect on water loss. The bare soil type encompasses a small area; therefore, the changes in the submerged depth at the five points in Fig. 4d are similar.

There was an upper limit to the water volume carried by the building roof in Fig. 4e, and the limit was determined by the roof structure. This finding supports the feasibility of green roofs in water regulation and storage. In Fig. 4f, we mainly focus on the points with obvious water accumulation. The submerged depth was 0 mm at points 2 and 4 in Fig. 4f, indicating that the drainage capacity of these sites matched the rainfall that accumulated throughout the whole process. The submergence depths changed at points 1, 3 and 5, and we can accurately locate them to help solve the drainage problem in time.

According to the above analysis, we marked the locations of rainwater gates that experiences drainage difficulties, as shown in Fig. 5.

The accumulated water running over the rainwater gates in Fig. 5 existed for at least one hour during this rainfall event, and the final submerged depths are shown in Fig. 5. Most of the rainwater gates that experiences drainage difficulties in the northwest and southeast corners of the study area, which caused regional waterlogging. According to the simulation results, corresponding drainage measures could be taken to alleviate waterlogging.

Section 2.2 shows that different land use types and scenarios correspond to different surface runoff generation processes. Six cells involved in at least three processes in

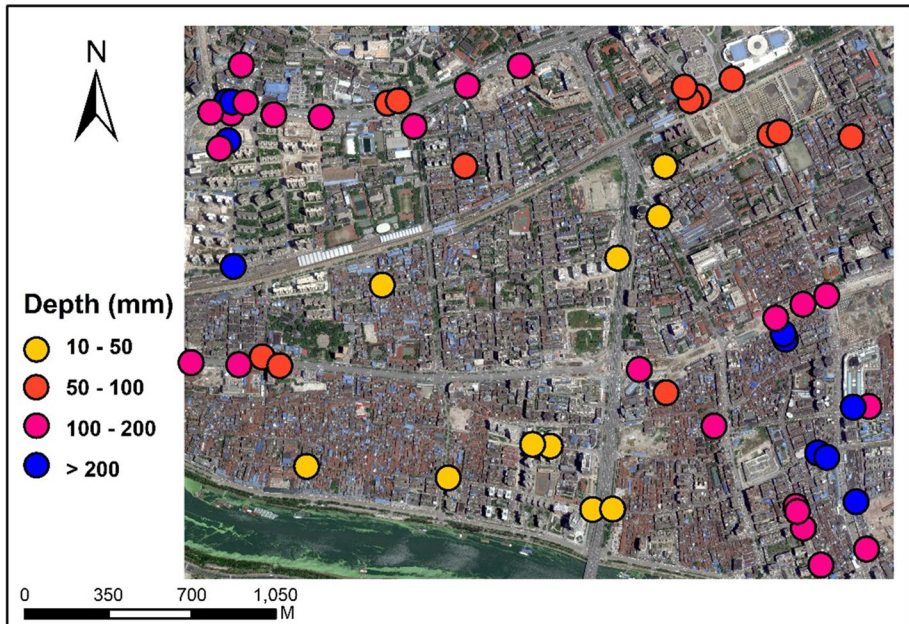


Fig. 5 The submerged depths over the rainwater gates when they had difficulty in drainage

runoff generation are selected; their submerged depths over time are recorded as shown in Table 2.

The terrain and LAI of the selected cells in Table 2 are relatively similar for comparison. Comparing the submerged depths of scenarios III and IV, the depression storage had a limited effect on reducing the amount of stagnant water. During heavy rain, areas with depressions will induce stagnant water or even faster waterlogging. The submerged depth of scenario VI shows that drainage facilities greatly alleviated the flooding situation. In summary, all processes in Table 2 indicate that vegetation interception and the infiltration of soil delayed the generation of accumulated water, and the final submerged depths were effectively reduced. Therefore, this discussion concludes that greening measures have a positive effect on urban flood alleviation.

4.3 Reduction of Surface Accumulated Water

Vegetation interception, infiltration and depression storage all have certain effects on water accumulation. We selected 20 sites with plants, where the processes of runoff generation involve rainfall, interception, infiltration and depression storage, to analyze the water storage capacity of different processes (Fig. 6).

When the total rainfall was 25 mm in Fig. 6a and 50 mm in Fig. 6b, the stagnated water resulting from vegetation interception and infiltration each accounted for approximately half of the total rainfall loss. With the increased rainfall shown in Fig. 6c and Fig. 6d, the effect of vegetation interception decreased, and the amount of depression storage increased. The stagnant water of the infiltration accounted for the largest proportion of rainfall loss. This shows that vegetation interception and infiltration are the main processes that reduce surface runoff during light or moderate rain; the effect of vegetation interception is limited during heavy rain, while the depression storage plays a gradual role, and infiltration always has a positive effect on runoff loss. To some extent, the results in Fig. 6 confirm the effectiveness of sponge city measures, such as the installation of permeable bricks and concave-down greenbelts.

4.4 Model Deficiency

This study focused on accurate inundation analysis under various land uses, and did not discuss the sensitivity of RRCA to different parameters, such as the time step.

Table 2 The submerged depth changes with time in six cells, where the runoff generation involves in at least three processes

Underlying surface types	Submerged depth (mm)					
	47 min	94 min	109 min	118 min	229 min	300 min
I Soil and depression	0	20.7710	43.1249	58.9906	137.963	210.076
II Vegetation and impervious depression	0	22.2987	44.2526	60.0183	138.890	210.903
III Vegetation and soil	0	0.6984	19.2524	32.9781	86.6908	142.6375
IV Vegetation, soil and depression	0	0	8.7801	22.5058	76.2185	132.1652
V Vegetation and building	0	18.5810	19.1410	19.1410	19.1410	19.1410
VI Vegetation and rainwater grate	0	0	0	0	0	0

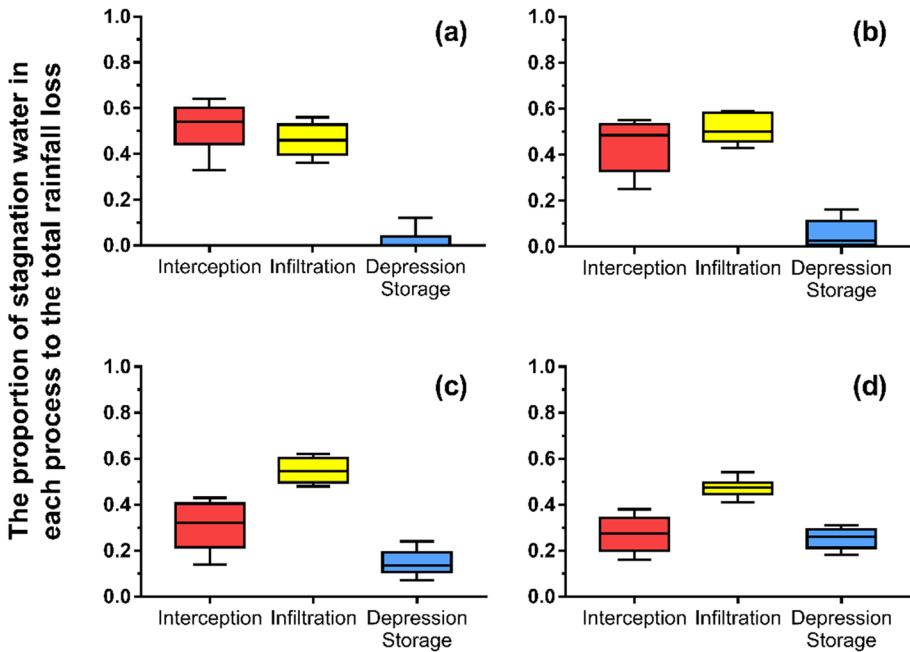


Fig. 6 The proportion of stagnated water in interception, infiltration and depression storage processes to the total rainfall loss when the rainfall is (a) 25 mm, (b) 50 mm, (c) 100 mm, and (d) 250 mm in one hour

In addition, RRCA is more suitable for the simulation of fine runoff processes at the neighborhood-scale, as the accuracy and efficiency can be guaranteed simultaneously in a small range. However, for large-scale flooding simulations, the efficiency of RRCA in this study is relatively limited by the lack of efficiency enhancement methods, such as cloud computing and edge computing.

5 Conclusion

It is difficult to simulate floods accurately in complex urban environments. To tackle this problem, this study proposes a new rainfall-runoff model based on CA (RRCA) for simulating the spatial and temporal evolution of inundation effectively. The simulation of RRCA considers multiple processes of runoff generation under various land uses and scenarios. The transition rules for water exchange are innovatively defined by the relationship between the water supply from center cell and the water demand of neighboring cells.

The comparison of RRCA and E2DCA shows that RRCA can identify stagnant water with a high accuracy and is more sensitive to the recognition of different waterlogging levels. The outputs include the distribution map of four waterlogging levels, the submerged depths with time and the locations experiencing drainage difficulties. This shows that once there is a continuous and heavy rain, the water-prone area will eventually cause severe flooding.

The submerged depths of various land use types and scenarios were analyzed based on multiple simulations. The results show that vegetation interception and infiltration have an effect on waterlogging prevention. In addition, accurate flood simulation can identify the key locations with drainage problems. The fine simulation of surface runoff and confluence processes can help researchers understand flood development, and RRCA will provide quantitative suggestions for urban greening and drainage system construction in waterlogging management.

Acknowledgements This work was supported by grants from the National Key Research and Development Program of China (No. 2018YFB2100500), the Fundamental Research Funds for the Central Universities (No. 2042020kf0011), the National Nature Science Foundation of China Program (No. 41771422, 41971351).

Authors' Contributions Shuang Yao: Writing—original draft preparation, Methodology, Software, Validation. Nengcheng Chen: Conceptualization, Supervision, Project administration. Wenyong Du: Writing—review and editing, Formal analysis. Chao Wang: Writing—review and editing. Cuizhen Chen: Data curation.

Funding This work was supported by grants from the National Key Research and Development Program of China (No. 2018YFB2100500), the Fundamental Research Funds for the Central Universities (No. 2042020kf0011), the National Nature Science Foundation of China Program (No. 41771422, 41971351).

Data Availability The data and materials are available except drainage network data.

Code Availability The code is available.

Declarations

Conflicts Of Interest/Competing Interests The authors declare that they have no known competing financial interests or personal relationships that could have appeared to influence the work reported in this paper.

References

- Almeida WS, Panachuki E, Oliveira PTS, Silva Menezes R, Sobrinho TA, Carvalho DF (2018) Effect of soil tillage and vegetal cover on soil water infiltration. *Soil Till Res* 175:130–138
- Alves A, Vojinovic Z, Kapelan Z, Sanchez A, Gersonius B (2020) Exploring trade-offs among the multiple benefits of green-blue-grey infrastructure for urban flood mitigation. *Sci Total Environ* 703:134980
- Armal S, Al-Suhili R (2019) An urban flood inundation model based on cellular automata. *Int J Water* 13(3):221–235
- Bennett ND, Croke BFW, Guariso G, Guillaume JHA, Hamilton SH, Jakeman AJ, Marsili-Libelli S, Newham LTH, Norton JP, Perrin C, Pierce SA, Robson B, Seppelt R, Voinov AA, Fath BD, Andreasian V (2013) Characterising performance of environmental models. *Environ Modell Softw* 40:1–20
- Bertsch R, Glenis V, Kilsby C (2017) Urban flood simulation using synthetic storm drain networks. *Water* 9(12):925
- Domeneghetti A, Schumann GJ-P, Tarpanelli A (2019) Preface: Remote Sensing for Flood Mapping and Monitoring of Flood Dynamics. *Remote Sens* 11(8):943
- Engman ET (1986) Roughness coefficients for routing surface runoff. *J Irrig Drain E-asc* 112(1):39–53
- Fassman-Beck E, Hunt W, Berghage R, Carpenter D, Kurtz T, Stovin V, Wadzuk B (2016) Curve Number and Runoff Coefficients for Extensive Living Roofs. *J Hydrol Eng* 21(3):04015073
- Gregorio SD, Serra R (1999) An empirical method for modelling and simulating some complex macroscopic phenomena by cellular automata. *Future Gener Comp Sy* 16(2):259–271
- Guidolin M, Chen AS, Ghimire B, Keedwell EC, Djordjević S, Savić DA (2016) A weighted cellular automata 2D inundation model for rapid flood analysis. *Environ Modell Softw* 84:378–394
- Guidolin M, Duncan A, Ghimire B, Gibson M, Keedwell E, Chen A S, Djordjevic S, Savić D (2012) CAD-DIES: a new framework for rapid development of parallel cellular automata algorithms for flood

- simulation, In: Pre-sented at the 10th International Conference on Hydroinformatics (HIC 2012), IWA (International Water Association, Hamburg, Germany)
- Hergarten S, Neugebauer HJ (1997) homogenization of Manning's Formula for modeling surface runoff. *Geophys Res Lett* 24(8):877–880
- Horton R E (1940) An approach toward a physical interpretation of infiltration capacity. *Soil Sci Soc Am J* 5(C):399–417
- Innovyze (2012) InfoWorks ICM Help v3.0
- Jamali B, Bach PM, Cunningham L, Deletic A (2019) A Cellular Automata Fast Flood Evaluation (CA-ffé) Model. *Water Resour Res* 55(6):4936–4953
- Jamali B, Löwe R, Bach PM, Urich C, Arnbjerg-Nielsen K, Deletic A (2018) A rapid urban flood inundation and damage assessment model. *J Hydrol* 564:1085–1098
- Lhomme J, Sayers P, Gouldby B, Samuels P, Wills M, Mulet-Marti J (2008) Recent development and application of a rapid flood spreading method. In: Samuels, P., Huntington, S., Allsop, W., Harrop, J. (Eds.), *Flood Risk Management: Research and Practice*. Taylor & Francis Group, London, UK.
- Li C, Fan Z, Wu Z, Dai Z, Liu L, Zhang C (2020) Methodology of Sub-Catchment Division Considering Land Uses and Flow Directions. *ISPRS Int Geo-Inf* 9(11):634
- Liu L, Liu Y, Wang X, Yu D, Liu K, Huang H, Hu G (2015) Developing an effective 2-D urban flood inundation model for city emergency management based on cellular automata. *Nat Hazards Earth Syst Sci* 15(3):381–391
- Manfreda S, Samela C (2019) A digital elevation model based method for a rapid estimation of flood inundation depth. *J Flood Risk Manag* 12(S1):e12541
- McCuen R, PA J, RM R (1996) *Hydrology, Hydraulic Design Series No. 2*, FHWA-SA-96-067, Federal Highway Administration, US Department of Transportation, Washington, DC
- Mishra SK, Tyagi J, Singh VP (2003) Comparison of infiltration models *Hydrol Process* 17(13):2629–2652
- Morbideilli R, Corradini C, Saltalippi C, Flammini A, Dari J, Govindaraju RS (2018) Rainfall infiltration modeling: a review. *Water* 10(12):1873
- Nazari M, Sadeghi SMM, Van Stan JT, Chaichi MR (2020) Rainfall interception and redistribution by maize farmland in central Iran. *J Hydrol: Regional Studies* 27:100656
- Rossman L, Huber W (2015) *Storm water management model reference manual volume I—Hydrology*. US Environmental Protection Agency, Washington, DC, USA
- Shang X, Jiang X, Jia R, Wei C (2019) Land use and climate change effects on surface runoff variations in the upper Heihe River basin. *Water* 11(2):344
- Shao Q, Weatherley D, Huang L, Baumgartl T (2015) RunCA: A cellular automata model for simulating surface runoff at different scales. *J Hydrol* 529:816–829
- Sun X (1999) *Drainage engineering (I)*. China Building Industry Press, Beijing
- Teng J, Jakeman AJ, Vaze J, Croke BFW, Dutta D, Kim S (2017) Flood inundation modelling: A review of methods, recent advances and uncertainty analysis. *Environ Modell Softw* 90:201–216
- Teng J, Vaze J, Kim S, Dutta D, Jakeman AJ, Croke BFW (2019) Enhancing the Capability of a Simple, Computationally Efficient, Conceptual Flood Inundation Model in Hydrologically Complex Terrain. *Water Resour Manag* 33(2):831–845
- Tyler J, Sadiq A-A, Noonan DS (2019) A review of the community flood risk management literature in the USA: lessons for improving community resilience to floods. *Nat Hazards* 96(3):1223–1248
- Uguz S, Akin H, Siap I, Sahin U (2016) On the irreversibility of Moore cellular automata over the ternary field and image application. *Appl Math Model* 40(17):8017–8032
- Vu TT, Law AWK, Nguyen TH, Chew AWZ (2019) Computational flood modeling with UPC architecture. *J Comput Civil Eng* 33(2):04019002
- Wolfram S (1984) Cellular automata as models of complexity. *Nature* 311(5985):419–424
- Zeng Z, Piao S, Lin X, Yin G, Peng S, Ciais P, Myneni RB (2012) Global evapotranspiration over the past three decades: estimation based on the water balance equation combined with empirical models. *Environ Res Lett* 7(1):014026
- Zhang S, Pan B (2014) An urban storm-inundation simulation method based on GIS. *J Hydrol* 517:260–268